Journal of Applied Polymer Science

Transparent Dispensible High-Refractive Index ZrO_2/Epoxy Nanocomposites for LED Encapsulation

Peng Tao, Ying Li, Richard W. Siegel, Linda S. Schadler
Department of Materials Science and Engineering, Rensselaer Polytechnic Institute, Troy, New York 12180
Correspondence to: P. Tao (E-mail: taop1985@gmail.com)

ABSTRACT: In this study, we report a facile *ex situ* approach to preparing transparent dispensible high-refractive index ZrO_2/epoxy nanocomposites for LED encapsulation. Highly crystalline, near monodisperse ZrO_2 nanoparticles (NPs) were synthesized by a nonaqueous approach using benzyl alcohol as the coordinating solvent. The synthesized particles were then modified by (3-glycidyloxypropyl)trimethoxysilane (GMS) ligand. It was found that, with tiny amount of surface-treating ligand, the modified ZrO_2 NPs were able to be easily dispersed in a commercial epoxy matrix because of the epoxy compatible surface chemistry design as well as the small matrix molecular weight favoring mixing. Transparent thick (1 mm) ZrO_2/epoxy nanocomposites with a particle core content as high as 50 wt % and an optical transparency of 90% in the visible light range were successfully prepared. The refractive index of the prepared composites increased from 1.51 for neat epoxy to 1.65 for 50 wt % (20 vol %) ZrO_2 loading and maintained the same high-Abbe number as the neat epoxy matrix. Compared with the neat epoxy encapsulant, an increase of 13.2% in light output power of red LEDs was achieved with the 50 wt % ZrO_2/epoxy nanocomposite as the novel encapsulant material. © 2013 Wiley Periodicals, Inc. J. Appl. Polym. Sci. 000: 000–000, 2013

KEYWORDS: compatibilization; composites; nanoparticles; nanowires and nanocrystals; optical properties; packaging

Received 13 March 2013; accepted 7 June 2013; Published online
DOI: 10.1002/app.39652

INTRODUCTION

Solid-state lighting, most commonly seen in the form of light-emitting diodes (LEDs), has the potential to revolutionize the efficiency, appearance, and quality of lighting.[1] Unlike conventional light sources, virtually all LED packages are encapsulated by a transparent polymeric material to help reduce the refractive index (RI) mismatch between the semiconductor LED dies and air, thereby improve the light-extraction efficiency.[2–7] High-RI encapsulant materials are needed to fundamentally alleviate the interface index mismatch and improve the efficiency of LEDs. Epoxy resins have been used as one of the most popular encapsulant materials for LEDs because of its good adhesion properties, mechanical robustness, and relative high-RI.[3,4,6,7] However, the RI of the most widely used bisphenol-A type epoxy encapsulant is limited below 1.55.[6,7]

Incorporation of high-RI nanoparticles (NPs) into epoxy resins has been pursued to effectively improve RI of the resultant nanocomposites.[8,9] However, most of the reported work has focused on thin films with a typical thickness less than 20 μm.[8,9] To be compatible with the current LED encapsulation design and processing, transparent dispensible thick (with a thickness up to 1 mm) nanocomposites are desired to form a dome-shaped encapsulant to fully extract the emitted light.[10] Technologically, *in situ* bulk polymerization of monomers initiated by γ-ray radiation or UV light has been used to prepare bulk transparent high-RI polymer nanocomposites.[11,12] However, the *in situ* polymerization technique has so far only been applied to limited types of polymers and this technique is not compatible with LED packaging processes. So far, the preparation of thick transparent dispensible epoxy-based nanocomposites via an *ex situ* method has not been previously reported. Moreover, the effectiveness of the high-RI nanocomposites on improving the light efficiency of LED packages has not yet been studied.

It is still a grand challenge to achieve stable dispersion of NPs within epoxy matrices by a simple method, although great efforts have been made in the past and limited success has been achieved only with filler concentrations less than 5 wt %.[13,14] To prepare transparent high-RI nanocomposites, the effective nanofiller-dispersing technology is the key. Typically, RI of the composites depends on the volume fraction of the high-RI filler. Because the high-RI inorganic fillers have a high density, usually a high loading (>30 wt %) is needed to effectively increase the RI of the nanocomposites.[15–18] Previously, we obtained good dispersions of poly(glycidyl methacrylate)-grafted TiO_2 NPs within epoxy matrices and achieved a 30 wt % particle-loading concentration.[16–18] Compared with the widely used high-RI

TiO_2 particles, ZrO_2 particles are less photocatalytic and are considered as more stable RI booster for polymers.[19] In the present work, we report the preparation of transparent bulk epoxy nanocomposites with a high-loading concentration (50 wt %) of ZrO_2 NPs by a simple and industrially more attractive route. Our approach combines the surface chemistry of the as-synthesized NPs with an effective postsynthesis surface ligand treatment to compatibilize the modified ZrO_2 NPs with a commercial epoxy matrix. We have successfully prepared colorless thick (1 mm) ZrO_2/epoxy nanocomposites. The optical properties (RI, transparency) and thermal stability of the nanocomposites were thoroughly characterized. Finally, we demonstrated that compared with the commercial epoxy-encapsulated LED, the prepared high-RI ZrO_2/epoxy nanocomposites with a RI of 1.65 increased the light output of red LEDs by 13.2%.

EXPERIMENTAL

Materials

Zirconium (IV) isopropoxide isopropanol complex and benzyl alcohol (anhydrous, 99.8%) were purchased from Alfa Aesar and Sigma-Aldrich, respectively. GMS was ordered from Gelest. Epoxy kit 301-1 was purchased from Epoxy Technology.

Surface Modification of ZrO_2 NPs

ZrO_2 NPs were synthesized via a nonaqueous synthetic route based on the procedure previously reported by Garnweitner et al.[20] In a typical synthesis, 2.22 g of zirconium isopropoxide isopropanol complex was dissolved in 30 mL of benzyl alcohol, and the mixture was transferred to a 45 mL stainless steel pressure vessel (Parr), which was heated to 240°C for 4 days. The as-synthesized milky ZrO_2 NP suspension within benzyl alcohol was subjected to a high-speed centrifugation (10,000 rpm) for 10 min. Then the precipitated particles were immediately dispersed into tetrahydrofuran (THF). Typically, 0.7 g of the as-synthesized ZrO_2 NPs was dispersed into 20 mL of THF. Subsequently, 200 μL of GMS was added into the dispersion and the dispersion, which was then sonicated at room temperature for 30 min. After sonication, the dispersion changed from milky to transparent. The mixture was further subjected to a high-speed centrifugation to obtain a transparent dispersion of modified ZrO_2 particles in THF.

Preparation of ZrO_2/Epoxy Nanocomposites

The obtained transparent ZrO_2 NP dispersion (20 mL) was put into a vacuum oven to remove the solvent at room temperature and was condensed to a solution of 5 mL. Then, diglycidyl ether of bisphenol-A epoxy resin (epoxy 301-1 part A) was added into the dispersion and the mixture was subjected to a final solvent removal process in a vacuum oven overnight. Finally, the curing agent (epoxy 301-1 part B, trimethyl-1,6-hexanediamine) was added into the mixture at a weight ratio of 1:4 with the resin part A. The resultant mixture was drop cast onto glass substrates followed by thermal curing at 80°C for 45 min.

Measurement and Characterization

Powder X-ray diffraction (XRD) patterns for ZrO_2 NPs were recorded with a PANalytical X'Pert Pro Diffractometer using Cu Kα radiation ($\lambda = 1.5405$ Å) in the 2θ range from 20 to 100° (step of 0.01°). Fourier transform infrared (FTIR) spectra were obtained on a PerkinElmer Spectrum One FTIR Spectrophotometer scanning from 450 to 4000 cm^{-1} with a resolution of 4 cm^{-1} for 10 scans. Thermogravimetric analysis (TGA) was done on a PerkinElmer Series 7 instrument. The sample was heated from 30°C to 700°C under a 90 mL min^{-1} nitrogen flow at a heating rate of 10°C/min. Transmission electron micrographs were obtained using a JEOL-2010 transmission electron microscope (TEM) operating at 200 kV. TEM samples were prepared by embedding ZrO_2/epoxy nanocomposites into a microscopy epoxy matrix and cutting the embedded composites into 50 nm slices at room temperature with a RMC PowerTome microtome.

RI dispersions of neat epoxy and ZrO_2/epoxy nanocomposites were measured on a variable angle spectroscopy ellipsometer (VASE, J.A. Woollam Co., Inc., Lincoln, NE) at three different incident angles (65, 70, and 75°) on a spin-coated sample on a Si wafer. The measured results were fitted with the Cauchy model with a typical mean square error less than 5. Transmittance spectra of the neat epoxy and ZrO_2/epoxy nanocomposites on glass substrates were measured with a Perkin-Elmer Lambda 950 UV–vis–NIR spectrophotometer using air as the reference. Neat epoxy and 50 wt % ZrO_2/epoxy nanocomposites were dispensed onto unencapsulated LED packages (PR2N-1LRS package on MCPCB, provided by ProLight Opto Technology Corporation) with the same bin of LED dies forming a dome. The encapsulants were then cured by placing the encapsulated LED package on a hotplate at 100°C for 30 min. The light-emission spectra and light-emission efficiency of unencapsulated LED packages, LED packages encapsulated with neat epoxy and with 50 wt % ZrO_2/epoxy nanocomposites were measured within an integrating sphere.

RESULTS AND DISCUSSION

Characterization of Synthesized Particles

Figure 1(a) shows a TEM image of the homogeneously dispersed as-synthesized ZrO_2 NPs on a copper grid. The particle size distribution was obtained using Image J by counting at least 200 particles from the TEM image. As shown in Figure 1(b), the particles exhibit a narrow size distribution with an average diameter of 3.8 nm. The uniform particle size distribution should be attributed to the slow reaction rate of the nonaqueous synthetic route as well as to the stabilization effect from the benzyl alcohol coordinating solvent.[20] The XRD pattern in Figure 1(c) indicates that the synthesized particles are highly crystalline and all the diffraction peaks can be assigned to the cubic zirconia phase (JCPDS No: 49–1642).[21] The sealed reaction condition within the pressure vessel and high reaction temperature at 240°C favor high crystallinity, thereby ensuring the high-RI feature of the synthesized ZrO_2 particles as filler materials. Based on the broadening of the (111) diffraction peak, using the Scherrer's equation, the size of the NPs was calculated to be 3.8 nm, which is the same value as that estimated from the TEM image. Figure 1(d) shows that the as-synthesized particles formed a milky dispersion within THF. Also shown by the photograph in Figure 1(d), the synthesized ZrO_2 particles are white powders after the removal of the THF solvent. Therefore, the small particle size, uniform size distribution, high crystallinity, and potentially better stability features

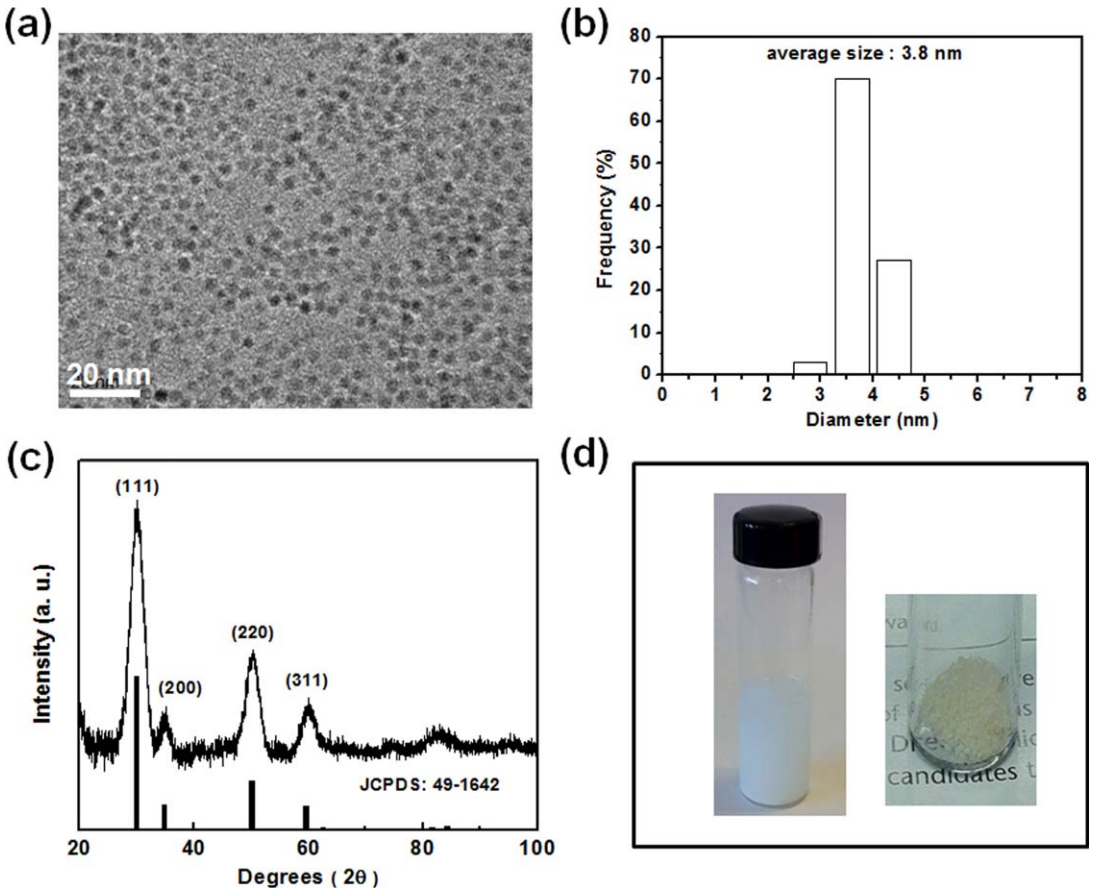

Figure 1. Characterization of as-synthesized ZrO_2 NPs: (a) TEM image; (b) particle size distribution measured by Image J software; and (c) XRD pattern; (d) appearances of the wet particle dispersion within THF and dry powders after removal of solvents. [Color figure can be viewed in the online issue, which is available at wileyonlinelibrary.com.]

enabled ZrO_2 NPs to be used as one of the most desired high-RI nanofillers.[22] Another important feature of this nonaqueous synthetic approach is the ease of scaling up production of high-quality particles by simply using a large volume pressure vessel.

The ZrO_2 NPs were obtained via a condensation reaction of zirconium isopropoxide precursor within benzyl alcohol, which involves a ligand exchange and an ether elimination process.[20] After the reaction, the particle surfaces were decorated with benzylmethoxyl species because of the condensation reaction between zirconium isopropoxide precursor and benzyl alcohol. It was reported that the benzyl alcohol solvent could also be adsorbed onto the as-synthesized particles via hydrogen bonding with surface hydroxyl groups.[23] The attached benzyl alcohol has a bulky phenyl group that can provide weak surface stabilization. However, without introducing additional ligands, the as-synthesized ZrO_2 particles cannot be dispersed within THF as evidenced by the milky dispersion shown in Figure 1(d).

Surface Mof ZrO_2 NPs

The TGA curve in Figure 2 reveals a 10% weight loss of the as-synthesized ZrO_2 particles because of the decomposition of the bound organic component. Two distinctive stages of weight loss were observed. The weight loss stage below 300°C can be attributed to physically adsorbed hydroxyl and organic volatiles, while the other stage above 300°C can be because of chemisorbed organic groups (including benzylmethoxyl and benzoate species).[24] Even after being washed three times with THF, there was no change in weight loss above 300°C indicating that the benzyl alcohol was chemically bound onto the ZrO_2 particles. FTIR spectrum of the as-synthesized ZrO_2 particles in Figure 3

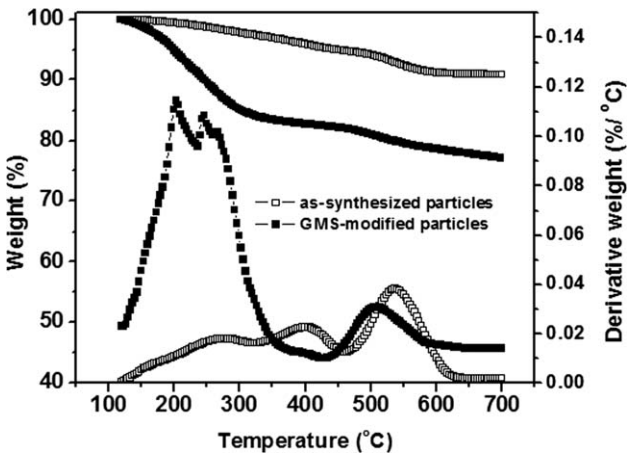

Figure 2. TGA curves of the as-synthesized and GMS-modified ZrO_2 NPs.

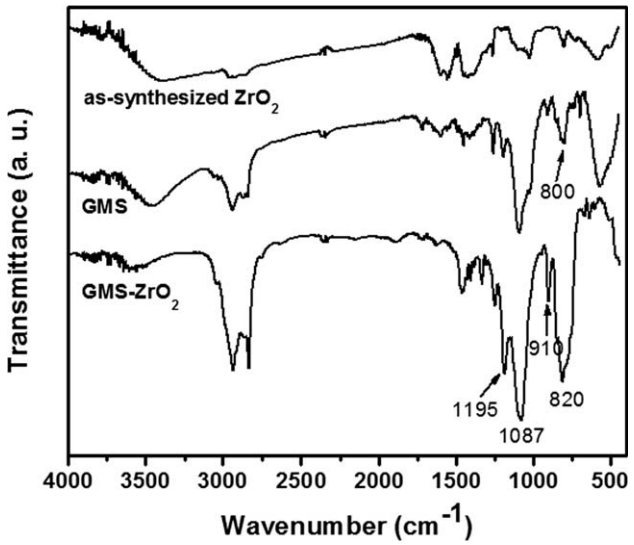

Figure 3. FTIR spectra of the as-synthesized, GMS treating agent and GMS-modified ZrO_2 NPs.

shows that in addition to the characteristic absorption band at 500–600 cm^{-1} associated with the Zr–O bond, the absorption bands at 1400–1600 cm^{-1} assigned to the absorbed benzyl alcohol are observed. Surprisingly, with a minute amount of GMS ligand the dispersion turned transparent after sonication for 10 min. TGA curve in Figure 2 shows a 20 wt % weight loss for the GMS-modified particles. The successful modification of ZrO_2 particles was further demonstrated by characteristic peaks of the epoxy ring at 910 and 1195 cm^{-1}. Compared with the characteristic silanol peak at 820 cm^{-1} in the FTIR spectrum of GMS, the stretching vibration peak shifted to 800 cm^{-1} after the formation of the Si–O–Zr bond. The other silane distinctive band at 1087 cm^{-1} is because of the asymmetric Si–O–Si stretching. These peaks indicate that GMS is chemically bonded onto ZrO_2 particles via the condensation between the methoxyl group from GMS and the hydroxyl groups on the particle. It was also noticed that the benzyl alcohol characteristic peaks in the range of 1400–1600 cm^{-1} are still present on the GMS-modified ZrO_2 particles. As shown by the TGA curve, the weight loss around 500°C associated with the decomposition of benzyl alcohol was also observed in the GMS-modified ZrO_2 particles.

The modified ZrO_2 particles were decorated with epoxy functional groups enabling them to be compatible with the epoxy matrix. The miscibility and dispersion of the surface-modified particles within polymer matrices are affected by their enthalpic compatibility and mixing entropy with the matrix polymers.[25,26] The mixed phenyl groups from the adsorbed benzyl alcohol and epoxy groups from the covalently bonded GMS ligands provide sufficient chemical similarity with the bisphenol-A epoxy matrix (Figure 4). Furthermore, the commercial epoxy matrix has a small molecular weight (~340 g mol^{-1}) which favors mixing and wetting with the GMS-modified ZrO_2 particles. Practically, in order to improve the refractive index of the nanocomposites, it is imperative to minimize the amount of grafted ligand and thereby realize high loading of the high-RI particle cores. Assuming an average area of 24 $Å^2$ per OH surface group (a graft density of 4 chain/nm^2), it would require 30 wt % of GMS to fully cover the ZrO_2 particle surfaces, if only one surface hydroxyl group was considered to react with each GMS ligand. If all the three methoxyl groups from the GMS ligand react with three hydroxyl groups on the particle surface, 10 wt % GMS ligand would be enough to modify the ZrO_2 particles. As mentioned before, some of the hydroxyl groups on the as-synthesized particles were coupled with benzyl alcohol, meaning that there will be a limited number of hydroxyl groups available for the reaction with GMS ligands. Experimentally, we achieved transparent dispersions of ZrO_2 particles within bisphenol-A epoxy matrix with less than 10 wt % GMS ligand, enabling the preparation of transparent nanocomposites filled with very high ZrO_2 particle loading.

Dispersion of ZrO_2/Epoxy Nanocomposites

Figure 4 shows that the GMS-modified ZrO_2 NPs formed a stable, colorless dispersion within the epoxy matrix after thorough removal of the solvent. After adding cross-linking agent, the nanocomposite can be easily applied onto a glass substrate and be dispensed onto the LED package. Figure 5 presents TEM images of ZrO_2/epoxy nanocomposites filled with GMS-modified ZrO_2 particles at 10, 30, and 50 wt % loading of particle cores (10.4, 30.6, and 46.8 wt % determined from TGA

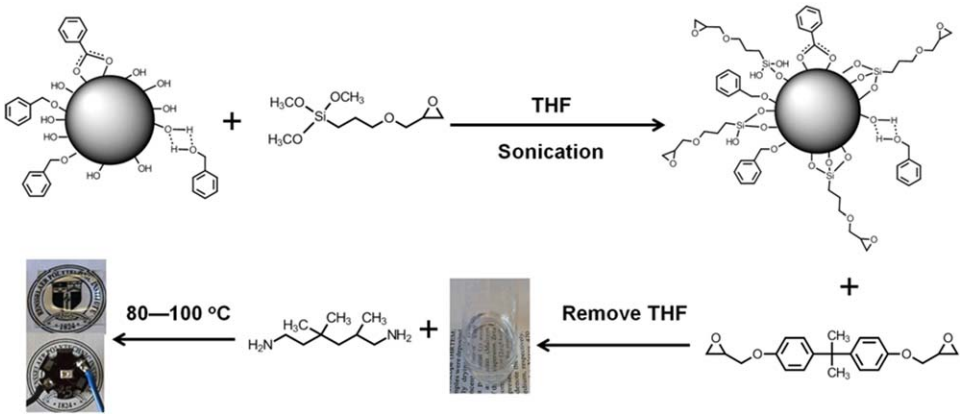

Figure 4. Illustration of surface modification of as-synthesized ZrO_2 NPs with GMS ligand and preparation process of ZrO_2/epoxy nanocomposites. [Color figure can be viewed in the online issue, which is available at wileyonlinelibrary.com.]

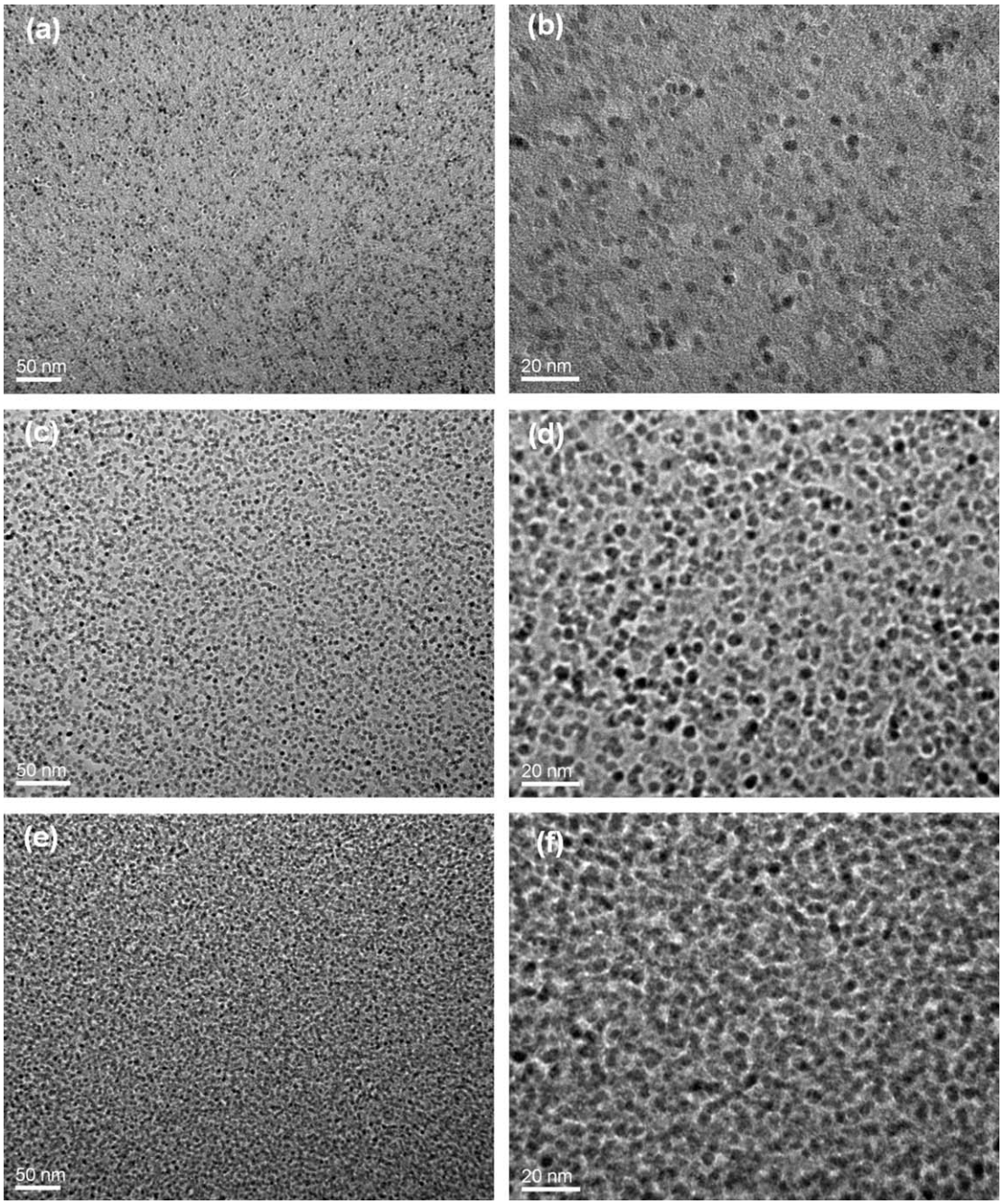

Figure 5. TEM images of ZrO_2/epoxy nanocomposites with different loading concentrations of ZrO_2 NPs under low and high magnifications: (a, b) 10; (c, d) 30; and (e, f) 50 wt %.

measurement) under low and high magnification. The ZrO_2 particles are homogeneously dispersed within the epoxy matrix without any observable agglomerates. It can be seen that with higher filler loading the particles are more densely distributed but without forming any clusters. As demonstrated by the TEM image at a high magnification, the GMS-modified ZrO_2 particles were randomly dispersed. Within the 50 wt % loading concentration sample, it can be seen that the ZrO_2 particles are so closely packed that they start to connect with one another. Surprisingly, the prepared nanocomposites are still highly transparent. This observation further highlights the importance of the uniform dispersion of NPs in suppressing scattering losses and achieving high optical transparency of the nanocomposites. Moreover, effective surface modification with tiny amount of the GMS ligands enables the high particle core loading in the final nanocomposites.

Optical Properties of ZrO_2/Epoxy Nanocomposites

Figure 6(a) shows the RI dispersion of the ZrO_2/epoxy nanocomposites in the wavelength range of 400–800 nm fitted by the Cauchy model, which expresses the refractive index as $n(\lambda)=A_n+\frac{B_n}{\lambda^2}+\frac{C_n}{\lambda^4}$, where λ is the wavelength, A_n, B_n, and C_n

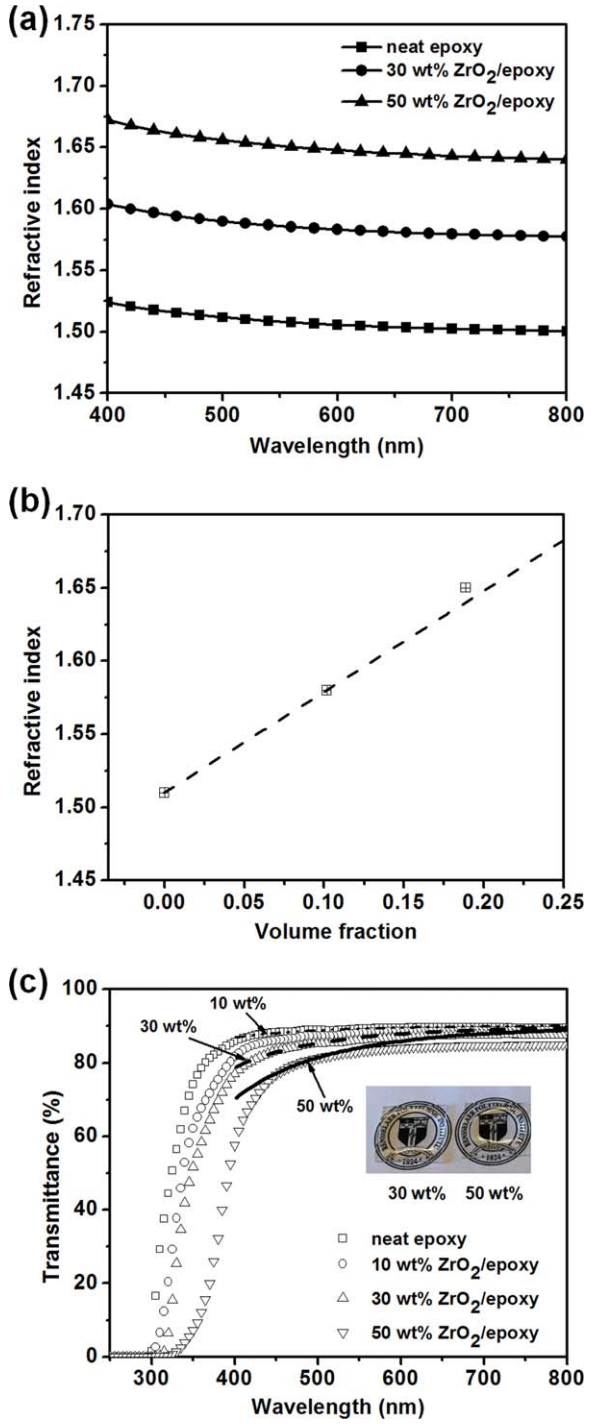

Figure 6. Optical properties of ZrO_2/epoxy nanocomposites: (a) RI dispersion; (b) dependence of RI at 600 nm on loading fraction of ZrO_2 NPs; and (c) transmittance spectra. The dash dot, dash line, and solid lines are the calculated transmittance spectra from the Rayleigh scattering model. The inset shows the appearance of colorless nanocomposites on a glass substrate. [Color figure can be viewed in the online issue, which is available at wileyonlinelibrary.com.]

are constants. As revealed in the following section, because of the high optical transparency of the nanocomposites in the visible light 400–800 nm range, there is essentially no absorption loss and ellipsometery measurement shows the imaginary part (k) of RI is almost zero. When measured by ellipsometer, the imaginary part of the RI was approximated to be zero and only the real part was listed. The RI of the nanocomposites increases from 1.51 for the neat epoxy matrix to 1.58 and 1.65 for the 30 and 50 wt % core loading concentrations, respectively. Assuming that the ZrO_2 particle and epoxy matrix have a density of 5.68 and 1.5 g cm^{-3}, respectively, 30 and 50 wt % loading concentration correspond to 10 and 20.1 vol %, respectively. As indicated by Figure 6(b), the RI of the nanocomposites at 600 nm shows a good linear dependence with the volume fraction of the ZrO_2 filler particles with the assumption that the RI of particles being 2.2. This is also consistent with our previous experimental results in homogeneously dispersed TiO_2 nanocomposites.[16] Theoretically, Maxwell–Garnett theory was used to model the RI dependence of composites filled with homogeneously distributed monodispersed spherical particles. Effective medium theory such as Bruggeman model further relaxed the requirement of filler particle size distribution in the composites.[27] However, as pointed out by Rao et al.,[28] generally the linear approximation is a good estimation for nanocomposites with good dispersion especially at low volumetric filler loading concentrations. Careful examination of the slope of the refractive index dispersion reveals that all the nanocomposites have a high-Abbe number (around 50) close to that of the neat epoxy matrix. Typically, incorporation of high-RI NPs sacrifices the Abbe number of the nanocomposites. The high-Abbe number of the prepared ZrO_2/epoxy nanocomposites should be ascribed to the high intrinsic Abbe number of ZrO_2 particles.[21] A large Abbe number means low optical dispersion and smaller chromatic aberration. The ZrO_2/epoxy nanocomposites would overcome the shortcoming of other high-RI nanocomposites and would have wider and more important applications as optical materials for such as lenses, prisms, and waveguides.[29]

Figure 6(c) presents the transmittance spectra of the 1 mm thick neat epoxy and ZrO_2/epoxy nanocomposites with different loadings on a glass substrate. The inset pictures show the appearance of the prepared 1 mm thick colorless 30 and 50 wt % ZrO_2/epoxy samples. Neat epoxy shows a transparency of 90% in the whole visible 400–800 nm range and a sharp UV cutoff at 300 nm. After the incorporation of ZrO_2 particles, the nanocomposites demonstrate enhanced UV-shielding capabilities with increasing particle loadings. The 50 wt % ZrO_2/epoxy sample almost totally blocks the UV light between 300 and 400 nm. Unlike the well-known strong UV-absorbing TiO_2 and ZnO particles, ZrO_2 particles are not efficient UV-absorbers and ZrO_2 typically has a larger band gap (5–7 eV).[19,21] The weak UV-shielding effect of ZrO_2 particles was further evidenced by the slight decrease of the transmittance of the nanocomposites filled with 10 wt % ZrO_2 particles in the UV range. In the visible light range, the ZrO_2/epoxy nanocomposites maintained almost the same high transparency as the neat epoxy.

Despite numerous reported measurements of the optical transmittance of the high-RI nanocomposites, very few efforts have been made to analyze the scattering behavior of polymer nanocomposites, especially for the thick nanocomposites.[9] Possibly it is because of the lack of good dispersions of NPs and the broad

particle size distribution of the fillers. Chung et al.[19] reported that the scattering behavior of their ZrO_2/epoxy nanocomposites was more consistent with the Mie theory and the optical transparency of the nanocomposite deteriorated dramatically with increasing the thickness of the sample. This could be related with the formation of particle clusters, which were observed in their composites. Given that the ZrO_2 particle size is much smaller than the wavelength of the incident visible light, here the Rayleigh scattering law was applied to understand the measured transmittance spectra in the visible light range. According to the Rayleigh scattering law,[30] the transparency for polymer nanocomposites can be described by eq. (1):

$$T_{PNC} = 0.9 \times \exp\left\{-\frac{32\pi^4 \varphi_p x r^3 n_m^4}{\lambda^4}\left[\frac{(n_p/n_m)^2 - 1}{(n_p/n_m)^2 + 2}\right]\right\} \quad (1)$$

where T_{PNC} is the transmittance of the nanocomposites, λ is the wavelength of the incident light, φ_p is the volume fraction of particles, r is the particle radius (1.9 nm), x is the optical path length (thickness of the sample, 1 mm), and n_p and n_m are the RI of the NPs (2.2) and the matrix (1.5), respectively. The dash dot, dash line, and solid line in Figure 6(c) present the predicted transmittance spectrum for 10, 30, and 50 wt% ZrO_2/epoxy nanocomposites. As shown by the overlapped transmittance spectra, the theoretical prediction from the Rayleigh scattering model agrees very well with the experimental measurements for 10 and 30 wt% loading sample. The slight deviation between experimental transmittance and theoretical prediction for the 50 wt % loading sample might be attributed to the increased reflection loss of the high-RI nanocomposites at the nanocomposite/air and nanocomposite/substrate interfaces. Compared with 30 wt % loading sample ($n = 1.58$), the 50 wt% ZrO_2/epoxy nanocomposites ($n = 1.65$) would have 2% more reflection loss.[31] Overall, the transmission behavior of the homogeneously dispersed ZrO_2/epoxy nanocomposites was reasonably well described by the Rayleigh scattering model. The good agreement should be attributed to the uniform dispersion, the near monodisperse particle size, and the relative small RI mismatch between the epoxy matrix and the ZrO_2 particles. The flat transmittance spectra further echo the homogeneous dispersion of the GMS-modified ZrO_2 NPs and the effective suppression of transparency loss because of scattering. The slight decrease of transparency in the high loading samples especially at low wavelength should be attributed to the inherent Rayleigh scattering loss.

Thermal Stability of Nanocomposites

Figure 7 shows the TGA curves for the neat epoxy and epoxy nanocomposites filled with 10, 30, and 50 wt % GMS-modified ZrO_2 NPs. All the ZrO_2/epoxy nanocomposites exhibit nearly the same good thermal stability as the neat epoxy matrix without significant weight loss up to 350°C in nitrogen. The neat epoxy matrix showed a very sharp degradation transition because of the optimized chemical composition. By contrast, the nanocomposite samples start to lose weight at temperatures above 200°C, although the weight loss is relatively small. The early stage weight loss and broader degradation transition is considered to be related to the adsorbed organic species from

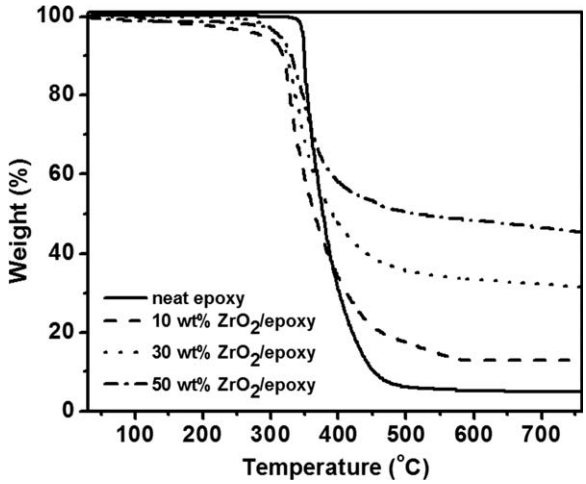

Figure 7. TGA curves of neat epoxy and epoxy nanocomposites filled with GMS-modified ZrO_2 NPs.

the added ZrO_2 particles and the disturbed cross-linking network of the epoxy matrix.[6,32]

In addition to the high-RI, high optical transparency, and good thermal stability features, LED encapsulant materials, especially those applied on high-brightness LEDs, also require good resistances against yellowing. Therefore, the ZrO_2/epoxy nanocomposites were subjected to an accelerated thermal aging test at 150°C for 24 h under an air atmosphere. As shown in Figure 8(a), after thermal aging, the neat epoxy and 10 wt% nanocomposite samples almost maintained the same transmittance spectra as before. However, the 30 and 50 wt % samples strongly absorbed the light in the range of 400–550 nm. The appearance of the samples changed from colorless to yellow as shown by the inset photographs. At higher loading concentrations, the 50 wt% sample showed a deeper yellow color. Epoxies were known for suffering yellowing issues especially after exposure to heat and short-wavelength light radiation. Both the bisphenol-A diglycidyl ether and amine-curing part are not thermally stable. For example, the bisphenol-A diglycidyl ether part can be easily oxided to form carbonyls, which essentially are chromophores. However, it is expected that ZrO_2 particles do not behave as traditional photocatalytic high-RI TiO_2 NPs accelerating decomposition of organic polymers. As pointed out by Bae et al.,[6,7] the yellowing of nanocomposites observed within high filler loading concentration samples might be related to insufficient cross-linking caused by the addition of GMS-modified ZrO_2 particles. The unreacted excessive epoxy groups or amine-curing agents as well as the adsorbed benzyl alcohol can act as sources of thermal oxidation and appear as yellowing. Therefore, optimizing the composition of the epoxy resin and curing agent in the nanocomposites would offer a potential solution to minimize the yellowness. Figure 8(b) plots the change of transmittance after aging. The absorptions of the low-wavelength visible light for the 30 and 50 wt % samples are obvious. Unlike the smooth spectra in Figure 6, some bumps were observed in the aged samples as shown in Figure 8(a). These bumps might be related with the change of surface roughness of the sample after the high-temperature aging

Applied Polymer SCIENCE

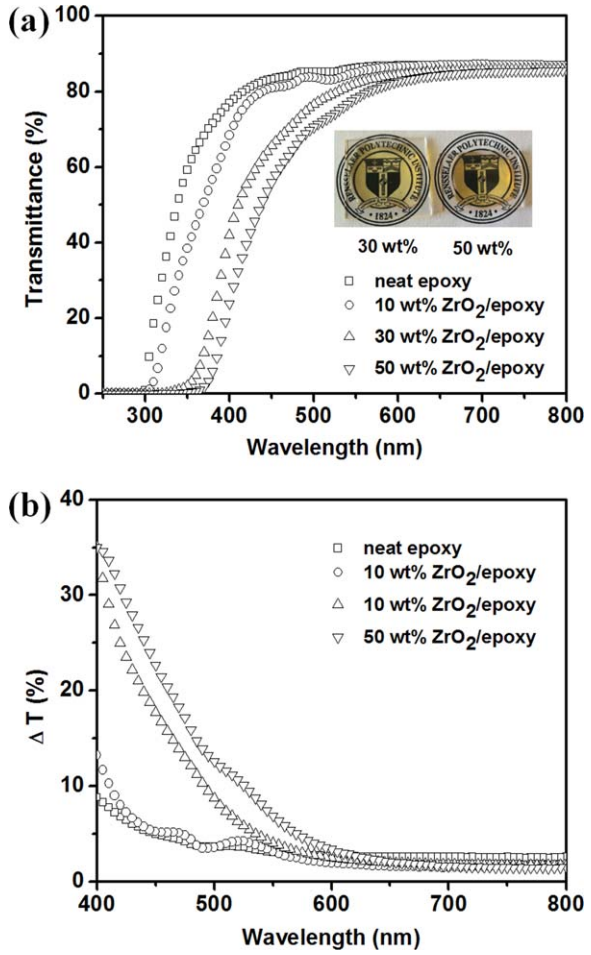

Figure 8. (a) Transmittance spectra and (b) transmittance change of neat epoxy and ZrO_2/epoxy nanocomposites with a thickness of 1 mm after thermal aging at 150°C for 24 h. The inset shows the appearance of transparent yellow nanocomposites on a glass substrate. [Color figure can be viewed in the online issue, which is available at wileyonlinelibrary.com.]

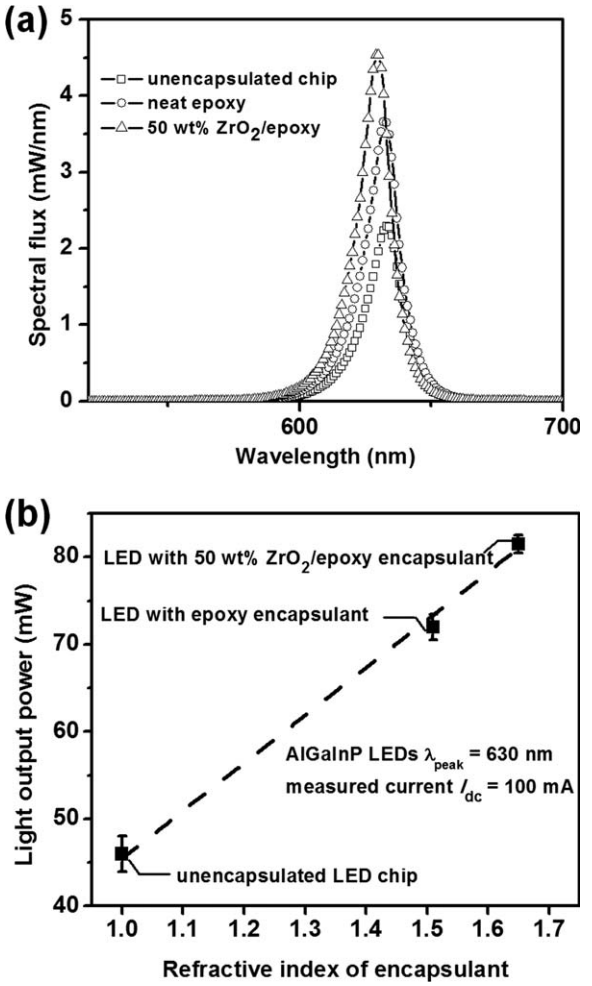

Figure 9. (a) Spectral scan of bare red LED chips and LED chips encapsulated with neat epoxy and ZrO_2/epoxy nanocomposites and (b) measured light output as a function of the RI of the encapsulant for red LEDs.

process. However, the ZrO_2/epoxy nanocomposites maintained essentially the same high optical transparency in the long wavelength 600–800 nm range after the thermal aging test.

Encapsulation of LED Packages

Considering the nondeteriorated transmittance at long wavelength range after thermal aging, the prepared high-RI ZrO_2/epoxy nanocomposites were used to encapsulate red LED packages. The homogeneously dispersed ZrO_2/epoxy nanocomposites maintained such good processability that they can be easily dispensed onto an LED package forming a well-defined dome-shape encapsulant. As shown by Figure 9(a), compared with unencapsulated LEDs, the encapsulated LEDs demonstrated higher light output and maintained the same symmetric emission peak centered around 630 nm. Integrating the area below the flux spectra yields the light output power. As shown in Figure 9(b), the LED light output power increases linearly with the refractive index of the encapsulant ($n_{encapsulant}$). After encapsulation with neat epoxy and ZrO_2/epoxy nanocomposites ($n = 1.65$), the light output increased by 56.6% and 77.2%, respectively. Compared with the LED encapsulated with commercial neat epoxy, the LED encapsulated with 50 wt% ZrO_2/epoxy nanocomposites showed an increase of 13.2% in light output. The previous 3D ray-tracing simulation carried out by Ma et al.[5] showed that, when $n_{encapsulant}$ is smaller than 2.0, the light-extraction efficiency increases quasi-linearly with $n_{encapsulant}$ for AlGaNInP red LEDs. The measured experimental results follow this theoretical prediction. Chung et al.[19] found that if the nanocomposites are translucent there was no obvious improvement of light intensity of LEDs. Owing to the homogeneous dispersion achieved by our approach, it is expected that the high-RI ZrO_2/epoxy nanocomposites could be used as new high-efficiency and stable encapsulant materials for red LEDs in the wavelength of 600–800 nm range and longer wavelength infrared LEDs. The future work would be to improve the stability of the nanocomposites against yellowing with optimized chemical compositions to enable them to be used as stable, high-efficiency encapsulant materials for blue LEDs as well.

CONCLUSIONS

In this work, we report a simple method to prepare bulk transparent high-RI ZrO_2/epoxy nanocomposites. With the

comprehensive control and understanding the surface chemistry of the synthesized ZrO_2 NPs and effective post surface ligand engineering, homogeneous dispersions of GMS-modified ZrO_2 NPs within a commercial epoxy matrix were achieved with a high ZrO_2 core content up to 50 wt %. All the bulk ZrO_2/epoxy nanocomposites demonstrated a high transparency (~90%) and their transmittance spectra were successfully described by a modified Rayleigh scattering model. The prepared nanocomposites also exhibited good thermal stability. Compared with the commercial neat epoxy encapsulant, the red LED package encapsulated with the 50 wt% ZrO_2/epoxy nanocomposites showed more than 10% increase in light output.

ACKNOWLEDGMENTS

This work was supported by the Engineering Research Center Program of the National Science Foundation under Cooperative Agreement EEC-0812056 and by NYSTAR under contracts C080145 and C090145. The financial support by the Nanoscale Science and Engineering Initiative of the National Science Foundation under NSF award number DMR-0642576 was acknowledged. The authors also thank the MRI award DMR 0821536 for supporting a multipurpose X-ray diffractometer and ProLight Opto Technology Corporation for supplying LED packages.

REFERENCES

1. Schubert, E. Light-Emitting Diodes; Cambridge University Press: Cambridge, **2006**.
2. Zhmakin, A.I. *Phys. Rep.* **2011**, *498*, 189.
3. Li, H.; Hsu, C.; Chen, K. 58th Electronic components and technology conference **2008**; p 1926.
4. Lin, Y.-H.; You, J.-P.; Lin, Y.-C.; Tran, N.-T.; Shi, F.-G. *IEEE Trans. Compon. Packag. Technol.* **2010**, *33*, 761.
5. Ma, M.; Mont, F.; Yan, X.; Cho, J.; Schubert, E. *Opt. Exp.* **2011**, *19*, 137.
6. Yang, S.; Kim, J.; Jin, J.; Kwak, S.; Bae, B. *J. Appl. Polym. Sci.* **2010**,*117*, 2140.
7. Yang, S.; Kwak, S.-Y.; Jin, J.; Kim, J.-S.; Choi, Y.; Paik, K.-W.; Bae, B.-S. *J. Mater. Chem.* **2010**, *22*, 8874.
8. Chau, J. L. H.; Tung, C.-T.; Lin, Y.-M.; Li, A.-K. *Mater. Lett.* **2008**, *62*, 3416.
9. Lü, C.; Yang, B. *J. Mater. Chem.* **2009**, *19*, 2884.
10. Luo, H.; Kim, J.-K.; Schubert, E.-F.; Cho, J.; Sone, C.; Park, Y. *Appl. Phys. Lett.* **2005**, *86*, 243505.
11. Lü, C.; Cheng, Y.; Liu, Y.; Liu, F.; Yang, B. *Adv. Mater.* **2006**, *18*, 1188.
12. Nakayama, N.; Hayashi, T. *Compos. Part A* **2007**, *38*, 1996.
13. Yang, Y.; Li, Y.; Fu, S.; Xiao, H. *J. Phys. Chem. C* **2008**, *112*, 10553.
14. Sun, D.; Sue, H.-J.; Miyatake, N. *J. Phys. Chem. C* **2008**, *112*, 16002.
15. Tao, P.; Viswanath, A.; Li, Y.; Rungta, A.; Benicewicz, B. C.; Siegel, R. W.; Schadler, L. S. *MRS Proc.* **2011**, *1359*, 163.
16. Tao, P.; Li, Y.; Rungta, A.; Viswanath, A.; Gao, J.; Benicewicz, B. C.; Siegel, R. W.; Schadler, L. S. *J. Mater. Chem.* **2011**, *21*, 8623.
17. Tao, P.; Viswanath, A.; Li, Y.; Siegel, R. W.; Benicewicz, B. C.; Schadler, L. S. *Polymer* **2013**, *54*, 1639.
18. Tao, P.; Viswanath, A.; Schadler, L. S.; Benicewicz, B. C.; Siegel, R. W. *ACS Appl. Mater. Interfaces* **2011**, *3*, 3638.
19. Chung, P.-T.; Yang, C.-T.; Wang, S.-H.; Chen, C.-W.; Chiang, A.; Liu, C.-Y. *Mater. Chem. Phys.* **2012**, *136*, 868.
20. Garnweitner, G.; Goldenberg, L. M.; Sakhno O. V.; Antonietti, M.; Niederberger, M.; Stumpe, J. *Small* **2007**, *3*, 1626.
21. Zhang, F.; Chupas, P. J.; Lui, S. L.A.; Hanson, J. C.; Caliebe, W. A.; Lee, P. L.; Chan, S. W. *Chem. Mater.* **2007**, *19*, 3118.
22. Althues, H.; Henle, J.; Kaskel, S. *Chem. Soc. Rev.* **2007**, *36*, 1454.
23. Hu, Y.; Gu, G.; Zhou, S.; Wu, L. *Polymer* **2011**, *52*, 122.
24. Luo, K.; Zhou, S.; Wu, L.; Gu, G. *Langmuir* **2008**, *24*, 11497.
25. Li, Y.; Tao, P.; Viswanath, A.; Benicewicz, B. C.; Schadler, L. S. *Langmuir* **2013**, *29*, 1211.
26. Tao, P.; Li, Y.; Siegel, R. W.; Schadler, L. S. *J. Mater. Chem. C* **2013**, *1*, 86.
27. Gehr, R. J.; Boyd, R. W. *Chem. Mater.* **1996**, *8*, 1807.
28. Rao, Y.; Chen, S. *Macromolecules* **2008**, *41*, 4838.
29. Liu, J., Ueda, M. *J. Mater. Chem.* **2009**, *19*, 8907.
30. Hiemenz, P. C.; Rajagopalan, R. Principles of Colloid and Surface Chemistry; Marcel Dekker: New York, **1997**.
31. Demir, M. M.; Koynov, K.; Akbey, Ü.; Bubeck, C.; Park, I.; Lieberwirth, I.; Wegner, G. *Macromolecules* **2007**, *40*, 1089.
32. Conley, R. T. Thermal Stability of Polymers; Marcel Dekker: New York, **1970**.